Dynamics of Transition to Enhanced Confinement in Reversed Magnetic Shear Discharges

P. H. Diamond,[1,*] V. B. Lebedev,[1] D. E. Newman,[2] B. A. Carreras,[2] T. S. Hahm,[3] W. M. Tang,[3]
G. Rewoldt,[3] and K. Avinash[4]
[1]*Dept. of Physics, University of California at San Diego, La Jolla, California 92093-0319*
[2]*Fusion Energy Division, Oak Ridge National Laboratory, Oak Ridge, Tennessee 37831*
[3]*Princeton Plasma Physics Laboratory, Princeton University, Princeton, New Jersey 08544*
[4]*Institute for Plasma Research, Bhat, Gandhinagar, 382 424, India*
(Received 5 March 1996)

A simple model of the transition to enhanced confinement in reversed shear discharges is presented. The proposed transition mechanism relies on a synergism between electric field shear suppression of turbulence aided by reduced curvature drive due to magnetic shear reversal or reduction. Profile structure and transport barrier propagation dynamics are predicted. A novel analytical theory for the time evolution of the barrier foot-point location is presented. The model predicts that the transition threshold has favorable dependence on pretransition temperature ratio (T_i/T_e), in-out asymmetry in the $E \times B$ shearing rate (i.e., lower for larger Shafranov shift), density profile peakedness, and unfavorable scaling with density. Optimal confinement occurs in discharges where deposition is peaked within the magnetic shear reversal radius. [S0031-9007(97)02457-5]

PACS numbers: 52.55.Fa

Achieving understanding and control of turbulent transport is a necessary prerequisite for the design of an economical advanced tokamak fusion reactor. Significant progress toward enhanced performance has been made by exploiting the spontaneous transition to high confinement regimes, such as *H* mode [1] or *VH* mode [2] induced by increased radial electric field shear. Such E_r shear [3], which is produced by the onset of sheared rotation and the steepening of the ion pressure profile, suppresses turbulence and transport [4], thus initiating a self-reinforcing feedback [5,6] which results in a bifurcation to a state with significant local reduction of fluctuations and transport. In *H* mode and *VH* mode, the transport barrier is initiated at the plasma edge.

Recently, a new regime of enhanced core confinement has been discovered in discharges with reversed magnetic shear [7,8]. In such discharges, formed by intense auxiliary heating of prelude (pretransition) plasmas during current ramp-up, confinement is observed to increase dramatically when a critical power input level is surpassed. Stored energy content builds rapidly, and a transport barrier forms at $r \gtrsim r_{\min}$, where $r_{\min}$ is the location of the minimum of $q(r)$. Typically, particle, ion thermal and momentum transport in the core of such ERS (enhanced reversed shear) [7] and NCS (negative central shear) [8] plasmas is reduced to levels below that of conventional neoclassical theory. This is consistent with the long standing predictions that negative magnetic shear will reduce geodesic curvature drive of microinstabilities [such as the toroidal ion temperature gradient (ITG) driven mode, various trapped particle modes, and high-*n* ballooning modes] and that peaked density profiles will quench ITG modes [9,10]. Nevertheless, the *theoretical* predictions that residual ITG turbulence and collisionless trapped electron mode turbulence should persist in prelude discharges [11], as well as the *experimental* indications of a clear bifurcation in particle, energy and momentum content evolution (as shown by a discontinuity in the time derivative of local density, ion temperature, and toroidal rotation velocity) *subsequent to establishment of reversed shear* all together suggest that *magnetic shear reversal is not sole cause of the remarkable confinement improvements observed in ERS/NCS-mode plasmas*. This is consistent with the observation of internal transport barriers in weakly negative shear discharges, where geodesic curvature drive is not fully eliminated [8].

Here, we propose a simple model of ERS/NCS transition dynamics. The model consists of an electric field shear driven transport bifurcation which develops in the radially inhomogeneous ambient transport environment characteristic of the prelude phase plasmas. The strong radial inhomogeneity is a consequence of the $q(r)$ profile structure. The essential mechanism intrinsic to the model is a *local* transport bifurcation which occurs when a local profile gradient threshold (entering the determination of E_r') is exceeded. Magnetic shear reversal lowers the local threshold, thus facilitating transition and localizing the region of barrier formation to the region of shear reversal. Thus, a *synergism* between the reduced curvature drive of the pretransition reversed shear plasma and the E_r'-driven transport bifurcation is *fundamental* to this model. The transition front is predicted to propagate [12] outward in radius until it reaches a radius at which the power, particle, or momentum input is insufficient to exceed the local threshold criterion. Note that within the scope of this model, the obvious question of why the *electric* field shear bifurcation is spatially pinned to the region of *magnetic* shear reversal is straightforwardly resolved, since (even weakly) negative shear significantly reduces geodesic curvature drive, thus lowering the *local* (electric field-shear-driven) bifurcation

 0031-9007/97/78(8)/1472(4)$10.00

threshold. Thus, magnetic and electric field shear effects are synergistic in our model.

The basic ERS/NCS dynamics can be manifested in a very simple two-field model which evolves local fluctuation intensity $\varepsilon(r,t) = \langle(\tilde{n}/n)^2\rangle$ and local mean density gradient magnitude $N(r,t) = |(1/\langle n\rangle)(d\langle n\rangle/dr)|$. Density gradient evolution is determined by the evolution of radially integrated mean density $\eta = \int_0^r dr'\langle n\rangle$. Thus, the basic equations are

$$\frac{\partial \varepsilon}{\partial t} = \frac{\gamma_0[(x - x_r)/\Delta_r]N\varepsilon}{1 + \alpha_2(r)(V_E'/V_c')^2} - \alpha_1(r)\varepsilon^2, \qquad (1a)$$

$$\frac{\partial}{\partial t}\eta = S(x/\Delta_d) - D_0\varepsilon N - D_n N. \qquad (1b)$$

Equations (1a) and (1b) are a generalization of a subset of previous models [4–6] to an inhomogeneous system. Here $\gamma_0[(x - x_r)/\Delta_r]N$ is the spatial profile of microinstability growth in the absence of electric field shear, Δ_r is the scale of variation in γ_0 about the geodesic curvature drive fall-off radius x_r, V_E'/V_c' is the normalized electric field shearing rate ($V_E'/V_c' \sim N^2$, from radial force balance), $S(x/\Delta_d) = 1/n\int_0^x dx' S_n(x')$. $D_0\varepsilon$ is the turbulent diffusivity, and D_n is the neoclassical diffusivity. Note $x = r^2$ is understood, and the geodesic curvature drive is reduced at x_r, but need not vanish. Also, $\alpha_1(r), \alpha_2(r)$ are model-dependent proportionality coefficients defined in Ref. [13]. Typical spatial profiles of $\gamma_0[(x - x_r)/\Delta_r]$ and $S_n(x/\Delta d)$ are shown in Figs. 1(a) and 1(b). Note that γ_0 decreases over a scale Δ_r in the neighborhood of x_r, and thus Δ_r corresponds to $(q''/q)^{-1/2}$, namely the characteristic width of shear variation. γ_0 is assumed small for $x < x_r$, corresponding to residual turbulence in the region of reversed shear. The profile of $S(x/\Delta_d)$ corresponds to an assumption of central deposition, with deposition profile width Δ_d.

The stationary condition for this model is thus simply

$$1 - \frac{D_n N(x)}{S(x/\Delta_d)} = \frac{D_0\gamma_0(x)N(x)^2/\alpha_1}{[1 + \alpha_2(N(x)^2)]S(x/\Delta_d)}. \qquad (2)$$

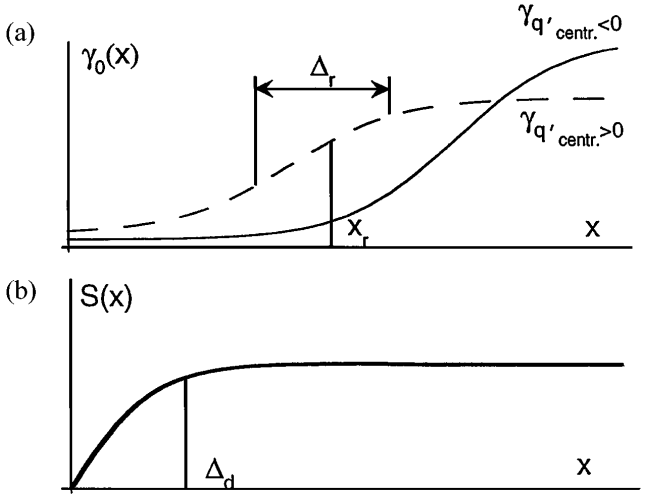

FIG. 1. (a) Spatial profile of turbulence growth rate. (b) Spatial profile of integrated deposition profile.

The solution of Eq. (2) determines the stationary profile of $N(x)$ in terms of the radially integrated deposition profile $S(x/\Delta_d)$ and the profile of the ambient transport in the prelude phase. Note that $N(x)$ is determined *locally* and exhibits a distinct prelude (i.e., *L*-mode-like) root when $\alpha_2(N^2)^2 \ll 1$, namely $N(x) = [\alpha_1 S(x)/D_0\gamma_0]^{1/2}$, and a steepened gradient (i.e., *H*-mode-like) root when $\alpha_2(N^2)^2 \gg 1$, namely $N(x) = S(x)/D_n$. In the latter case, the profile is determined by neoclassical transport alone. It is apparent from inspection that $N(x)$ will fall into the *H*-mode-like state for $x < x_r + \Delta_r$ where $\gamma_0[(x - x_r)/\Delta_r]$ is small and the *local* "$L \longrightarrow H$" transition threshold is easily exceeded. For $x_r + \Delta_r$, $\gamma_0(x)$ increases rapidly, so the solution for $N(x)$ must revert to a prelude phase value. Between these regions of asymptotic behavior, the boundary of the core transport barrier is located.

The nontrivial spatial structure of the stationary state profile is greatly elucidated by considering the surface of constant transport flux Γ (here $\Gamma = D_0\varepsilon N$) in the space of position and gradient (x, N). This *flux landscape* (drawn for TFTR parameters—see later) is shown in Fig. 2(a). Note that constant *N* slices of the flux landscape depict the familiar radial profiles of Γ and (implicitly) *D*, which increase with radius. Correspondingly, a constant-*x* slice of $\Gamma(x, N)$ traces an *S*-shaped bifurcation curve which describes the local gradient transition at each radial location. Two prominent features of the flux landscape are a steep ridge at modest values of *N*,

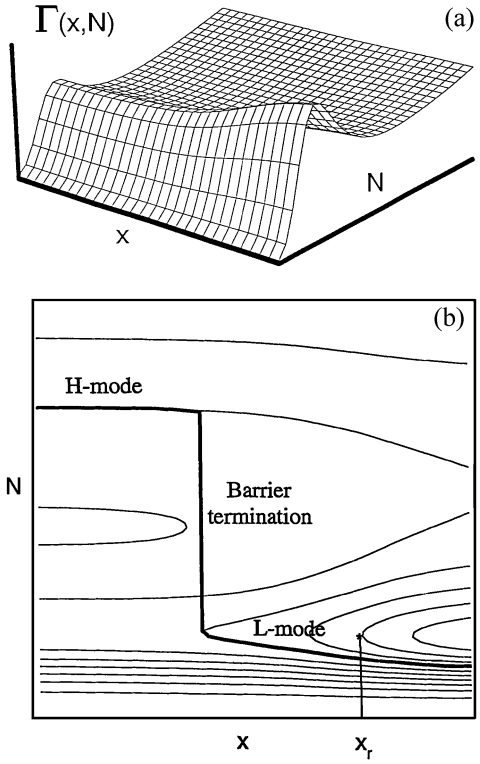

FIG. 2. (a) Transport flux landscape, in position-gradient space. (b) Topography of constant-Γ contours in position-gradient space.

which proceeds into a hill at large x and modest N. These are hereafter termed the prelude phase ridge and hill, respectively. At large N, a second, topographically simpler up-slope appears at all values of x. The slope of this inclination, dubbed the H-mode beach, is set by D_n, as the inclination is determined by neoclassical transport. The actual solution profile of $N(x)$ is determined by the intersection of the flux landscape with the deposition surface $S(x/\Delta_d)$, which is flat for $x > \Delta_d$, i.e., for radii beyond the deposition region. Thus the transport barrier lies in the region $\Delta_d < x < x_r$. This is shown in Fig. 2(b), which is a topographic plot of constant flux contours in x, N space. Note that the large-x boundary of the barrier is located where the prelude hill is high enough to intersect the deposition surface, thus causing $\Gamma(x, N)$ to be locally double valued. This determines a lower bound in x for the location of the catastrophe [14], representative of a local $H \rightarrow L$ transition. The precise location of the barrier foot-point must be determined using a dynamical calculation, given below. Note also that the structure of the flux landscape dramatically suggests that optimal performance will result when the deposition region is located within the shear reversal radius, i.e., $\Delta_d < x_r$. This is because particles or power deposited at $x > x_r$ will experience L-mode transport and thus suffer degraded confinement. These conclusions are consistent with experimental studies [15].

The dynamics of reversed shear discharge evolution may be studied numerically using a simple extension of the model of Eqs. (1a) and (1b), obtained by retaining radial transport to provide spatial coupling. The extended model equations are

$$\frac{\partial \varepsilon}{\partial t} = \gamma_0(x) N_\varepsilon - \alpha_1 \varepsilon^2 - \alpha_2 V_E'^2 \varepsilon + \frac{\partial}{\partial x}\left(D_0 \varepsilon \frac{\partial \varepsilon}{\partial x}\right), \tag{3a}$$

$$\frac{\partial N}{\partial t} = S - D_n N + \frac{\partial}{\partial x}\left(D_0 \varepsilon \frac{\partial N}{\partial x}\right). \tag{3b}$$

Here, the notation is that of Refs. [6,13]. The temporal evolution of N at various radii during a power ramp is shown in Fig. 3. A radially local discontinuity in dN/dt clearly occurs at progressively increasing radii, thus indicating a *local* gradient transition which propagates outward in radius as the power input rate is increased. This phenomenon has subsequently been identified in NCS discharge of DIII-D. The ultimate location of the transition front is determined by the input strength and the slope of the prelude phase hill of the $\Gamma(x, N)$ surface, as predicted in the previous paragraph.

The simplest possible model of ERS discharge *dynamics* is that defined by the nonlinear transport equation with bi-stable flux function $\Gamma(x, N)$, so that $\partial n/\partial t = -\partial \Gamma(x, N)/\partial x$. Here, $\Gamma(x, N)$ is s shaped at constant x, as are cross sections of Fig. 2(a). Note that this discussion does not assume the specific functional form of Γ used in Eq. (1). Then, the transport barrier foot-point location is

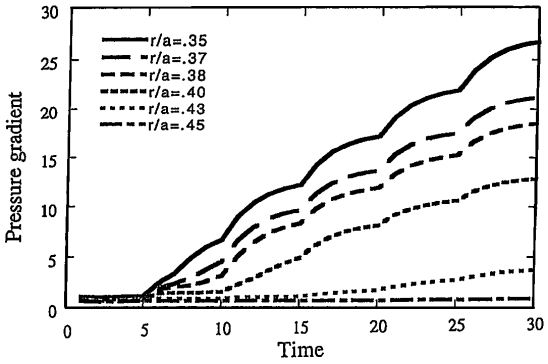

FIG. 3. Time histories of the pressure gradient at different radial locations during a power ramp.

given by $\ell(t)$, where $x < \ell(t)$ is the core region of collisional transport ($D = D_n$) and $x > \ell(t)$ is the region of anomalous transport ($D = D_a$). The transport bifurcation occurs in a narrow layer about $\ell(t)$. The trajectory history of $\ell(t)$ is determined by the matching conditions for the bi-stable transport bifurcation problem, which require continuity of density and particle flux, and also impose a condition akin to the Maxwell construction, familiar from phase equilibrium theory. The latter is obtained by multiplying the transport equation by n and integrating through the bifurcation front layer (of thickness δ), yielding

$$N\,\Gamma(N)\big|_{\ell_-}^{\ell^+} = \int_{N_-}^{N_+} dN\,\Gamma(N) \tag{4}$$

for a stationary state. Note that Eq. (4) is satisfied by a unique value of Γ, corresponding to transition from profile gradient N_- to N_+ at ℓ. This value is hereafter referred to as Γ_M. Then the matching conditions are then just $\Gamma_{\ell_-} = \Gamma_{\ell_+} = \Gamma_M$, $n(\ell_-) = n(\ell_+)$, and Eq. (4). Additional (edge) boundary conditions are $n(a) = 0$ and $\Gamma_0 = -D_{\text{neo}}\partial n/\partial x$ (Γ_0 is the flux from the core, assuming central deposition). Inspection of the resulting diffusion problem reveals that one cannot simultaneously satisfy the matching criteria at $x = \ell$ and the boundary conditions at $x = 0$, $x = a$ unless $\Gamma_0 = \Gamma_M$. Thus, Γ_M determines the particle fueling rate (more generally, power) required to sustain a stationary transport barrier with foot at $x = \ell$. Of course, the slope of the prelude phase hill determines Γ_M and thus the ultimate stationary value of ℓ. For $\Gamma_0 > \Gamma_M$, $\ell(t)$ will increase and the core N will steepen, until limited by other physical processes (i.e., stability to "infernal" modes [16]). When $\Gamma_0 \gtrapprox \Gamma_M$, so that $\dot{\ell}\ell < D_{\text{neo}}$, approximate solution of the time-dependent, nonlinear evolution problem for $\ell(t)$ yields

$$\ell(t) \cong \left[\left(\frac{\Gamma_0 - \Gamma_M}{\Gamma_M}\right)\left(\frac{D_a D_n}{D_a - D_n}\right)t\right]^{1/2} \cong \left(\frac{\Gamma_0 - \Gamma_M}{\Gamma_M}\right)^{1/2} D_n t^{1/2}. \tag{5}$$

Thus, the transport barrier foot-point position $\ell(t)$ increases diffusively at D_n. More generally, $\ell(t)$ evolves

according to $\ell(t) \sim [(P - P_{\rm crit}/P_{\rm crit})]^{1/2}(D_n t)^{1/2}$, where $P_{\rm crit}$ is the *local* power threshold for a transport bifurcation. These results are qualitatively consistent with those shown in Figs. 3(a) and 3(b). Further discussion and details of this derivation are given in Ref. [17].

The major quantitative question pertinent to describing the ERS/NCS transition is that of predicting the profile threshold required to trigger the bifurcation. In this simple model, the electric field shear is determined primarily by the density gradient, so the relevant threshold parameter is F, the particle input rate (i.e., $P_{\rm in}/\in_b$, where $\in_b$ is the energy per beam particle). In toroidal geometry [18], the $E \times B$ shear suppression criterion is $\omega_s = (\Delta\psi_0/\Delta\phi)\partial/\partial\psi\,[(cEr/RB_\theta)] > \Delta\omega_k$, where ψ is the flux coordinate and $\Delta\omega_k$ is the turbulent decorrelation rate. Here, $\Delta\phi$ is the toroidal correlation angle, $\Delta\psi_0 = RB_\theta\Delta r_0$, where Δr_0 is the radial correlation length of the turbulence. Using radial force balance (assuming ∇n controls E_r') and particle balance with the assumption of gyro-Bohm particle diffusion then yields the threshold criterion

$$\frac{F(\psi)}{A(\psi)} \geqq \langle n\rangle(\rho_s^2 c_s/\Delta r_0^2)\,\frac{\langle (RB_\theta)^3 f(\theta)\rangle}{\langle RB_\theta\rangle (RB_\theta)^2} \times \left(\frac{T_e}{T_i}\right)^2\left(\frac{\Delta\omega}{\omega_{*e}}\right)_{\bar{k}}^2. \quad (6)$$

Here $A(\psi)$ is the surface area defined by ψ. Note that the radial force balance and particle balance equations used to calculate E_r necessarily involve flux surface averaged quantities, which thus propagate into Eq. (6). However, ω_E itself is *not* a flux function and the shear suppression criterion is *not* a flux surface averaged criterion. The factor $(RB_\theta)^{-2}$ indicates an in-out asymmetry of the transition threshold, which is more strongly favorable with increasing Shafranov shift, and the $(T_e/T_i)^2$ factor arises from the presumption of collisionless trapped electron modes (CTEM) as the ambient turbulence of the prelude discharge. $f(\theta)$ is a dimensionless poloidal profile factor of order unity, and F is the rate of particle deposition within ψ for monotonically decreasing particle deposition profile. The most interesting features of Eq. (6) are its prediction of favorable dependence of F on T_i [via $(T_e/T_i)^2$], and on strong in-out asymmetry (i.e., lower threshold for larger Shafranov shift). Taking $\Delta\omega_k \sim \gamma_k$ (in lieu of $\Delta\omega_k$ measurements or calculations) and noting that the growth rate for CTEM scales as $\exp[-R/L_n]$ reveals that $F/A(\psi)$ decreases with increasing target density profile peakedness. In particular, transition appears easiest in hot ion, high β_ρ discharges with low B_θ, low current, and low density. Thus, hot ion mode plasmas such as super-shots appear to be optimal prelude discharges. Note also that the transition criterion appears naturally as an input-per-area threshold for local transition, assuming central fueling.

The simplest model presented here requires significant augmentation prior to use in predictive modeling. Specifically, ion temperature, toroidal and poloidal velocity, and current must be self-consistently evolved in shaped tokamak geometry. The target plasma profile dependence of the deposition function must be accounted for [i.e., $S = S(N, x/\Delta_d)$]. A partially augmented model, which evolves transport equations for n, T_i, T_e, and ε has already been developed. Solution of this model for TFTR parameters ($B_T = 4.7$ T, $R = 250$ cm, $a = 82$ cm, and $\Delta_d \cong 0.2a$) predicts an ERS transition at $P_{\rm crit} \cong 17$ MW, in good agreement with experimental results. In this case, the reversal radius was located at $0.35a$ and on-axis parameters of $T_i = 24$ KeV and $n = 5 \times 10^{14}$ cm^{-3} were calculated. These results are also in good agreement with experiment. It is interesting to note that while the initial transition location and behavior are sensitive to local growth rates and local gradients in $q(r)$ and power deposition, the global transition dynamics appear remarkably robust. These (and further) extensions of the model will be discussed in future publications.

We thank K. H. Burrell, M. Zarnstorff, M. Beer, L. Lao, H. Park, and E. Synakowski for useful discussions. This research was supported by U.S. DOE Contract No. DE-FG03-88-ER53275 (UCSD), U.S. DOE Contract No. DE-AC05-960R22464 (Lockheed Martin Energy Research Corp.), and U.S. DOE Contract No. DE-AC02-76-CHO-3073 (PPPL).

*Also, General Atomics, San Diego CA 92122.

[1] F. Wagner *et al.*, Phys. Rev. Lett. **49**, 1408 (1982).
[2] G. L. Jackson *et al.*, Phys. Rev. Lett. **67**, 3098 (1991).
[3] S.-I. Itoh and K. Itoh, J. Phys. Soc. Jpn. **59**, 3815 (1990).
[4] H. Biglari, P. H. Diamond, and P. W. Terry, Phys. Fluids B **2**, 1 (1989).
[5] F. L. Hinton, Phys. Fluids B **3**, 696 (1991); G. M. Staebler *et al.*, Phys. Plasmas **1**, 909 (1994).
[6] P. H. Diamond *et al., Proceedings IAEH 1994 meeting, Plasma Physics and Controlled Nuclear Fusion Research* (IAEA, Vienna, 1996), Vol. III, p. 323.
[7] F. M. Levinton *et al.*, Phys. Rev. Lett. **75**, 4417 (1995).
[8] E. J. Strait and L. L. Lao *et al.*, Phys. Rev. Lett. **75**, 4421 (1995); Y. Koide *et al.*, Phys. Plasma (to be published).
[9] B. B. Kadomtsev and O. P. Pogutse, Sov. Phys. JETP **24**, 1172 (1967).
[10] C. Kessel *et al.*, Phys. Rev. Lett. **72**, 1212 (1994); J. Y. Kim and M. Wakatani, Phys. Plasmas **2**, 1012 (1995).
[11] M. A. Beer *et al.*, Phys. Plasmas (to be published).
[12] P. H. Diamond *et al.*, Phys. Plasmas **2**, 3685 (1995).
[13] P. H. Diamond *et al.*, Phys. Rev. Lett. **72**, 2565 (1994).
[14] V. I. Arnol'd, *Catastrophe Theory* (Springer-Verlag, Heidelberg, 1984); I. Stewart, Physica (Amsterdam) **2D**, 245 (1981).
[15] H. K. Park *et al.*, Nucl. Fusion Lett. **34**, 1271 (1994).
[16] M. W. Phillips *et al.*, Phys. Plasmas **3**, 1673 (1996).
[17] V. B. Lebedev and P. H. Diamond, Phys. Plasmas (to be published).
[18] T. S. Hahm and K. H. Burrell, Phys. Plasmas **2**, 1648 (1995).